

# Sensorless DTC of an Induction Motor based on Intelligent Dual Observer and ANN based Selector Table

CHAYMAE FAHASSA<sup>1</sup>, MOHAMED AKHERRAZ<sup>2</sup>, ABDERRAHIM BENNASSAR<sup>3</sup>

Department of electrical engineering  
Mohammed V University, Mohammadia school of engineering (EMI)  
Avenue Ibn Sina PO 765, Agdal-Rabat  
Morocco  
Fahassa.chaymae@gmail.com

*Abstract:* - Several industrial applications require control techniques combining simplicity, robustness, and a good performance. In order to achieve this combination, the following infrastructure is proposed; a dual observer is used for our sensorless direct torque control (DTC) of a three-phase squirrel cage induction motor drive (SCIM), combining the adaptive luenberger observer (ALO) based on an intelligent hybrid technique for adaptation mechanism, and the extended Kalman filter (EKF), the first observer estimates the rotor speed while the second estimates the flux components; a proportional integral (PI) anti-windup controller which replaces the conventional speed PI controller; along with an intelligent approach namely artificial neural networks (ANN) based selector table in order to substitute the conventional one. The proposed structure, on one hand optimizes and reduces the torque, stator flux and stator current ripples, and on the other, provides an improved speed response characterized by a fast dynamic response, small overshoot, as well as resistance to disturbances. Simulation results prove the effectiveness and robust performance of the proposed sensorless intelligent strategy in both low and high speeds, direct and reverse directions, with and without applying a load disturbance.

*Key-Words:* - Artificial Neural Networks, Fuzzy Logic, Extended Kalman Filter, Adaptive Luenberger Observer, PI Anti-Windup, Sensorless Direct Torque Control, Induction Motor.

## 1 Introduction

The induction motor (IM) is considered the most favoured machine in industrial and household setting applications, thanks to the several advantages it offers, to cite a few : the simplicity, robustness, lower cost, reduced maintenance, high accuracy combined with low failure rate [1]. Furthermore, the progress power electronics has known made the wide-scale application of variable speed IM drives a reality. The main purpose behind induction motors control is to obtain an efficient performance employing the simplest possible control structure. DTC achieves these conditions. DTC patent is credited to Takahashi, Noguchi [2] and Depenbrock [3].

In DTC, direct control of the electromagnetic torque and stator flux is reachable through the selection of optimum inverter switching modes, which are generated by the selector table [4]. DTC, accommodates to a torque dynamic while avoiding vector control complexity, since it does not require voltage decoupling circuits and coordinate transformations, moreover it requires a minimum number of controllers [5].

Amongst DTC's main disadvantages the high torque and flux ripples, as well as a slow transient

response to the step changes in torque during start-up [6]. This inaccuracy of the stator flux and electromagnetic torque strongly influences DTC operation, especially during start-up and at the low speeds range. In order to eliminate these issues, an intelligent ANN based selector table is proposed to substitute the conventional one; ANN do not require any mathematical equations thanks to their ability of learning from processes and example data. They have the ability to learn the relationship between a set of input data and the corresponding output data. Thus, they memorize data and generalize this information when performing with a new input data by giving appropriate output data [7]. Furthermore, the ANN approach is efficient to approximate nonlinear functions.

Moreover, in order to enhance the stability and robustness of the system's dynamic, a speed PI anti-windup controller based on back calculation is inserted to correct the integral action [8]. This latter is characterized by its simple design and excellent dynamic.

In order to decrease hardware complexity [9], the speed sensor is eliminated in this paper, and a new robust sensorless technique is proposed; a hybrid observer mixing ALO for rotor speed estimation,

and EKF for the flux components estimation. The ALO is based on the intelligent hybrid adaptation mechanism which combines fuzzy logic (FL) and PI anti windup techniques. These combined techniques present many advantages; To cite a few: the capability of the fuzzy to transform human expert's knowledge, into an automatic control strategy [10], the integral action correction by the PI anti-windup, the stability of the ALO [11], as well as the reduction of problems related to parameter variations and noise in measurements which are inherently taken care by the EKF algorithm. These advantages allow accurate rotor speed, and flux components control.

The outline of this paper is as follows; it begins with an introduction; in the second section the asynchronous motor modeling is discussed. Section three reviews the direct torque control principle. The proposed artificial neural networks selector table is addressed as well in section four; the PI anti-windup speed controller is described in section five. Section six is devoted to the dual observer. Section seven covers simulation results and discussion. Finally, a conclusion is made along with the reference list.

## 2 Asynchronous Motor Modeling

The dynamic model of an IM in the stator reference frame,  $(\alpha, \beta)$  coordinates, can be expressed by the following state equations:

$$\dot{X} = AX + BU \tag{1}$$

Equation (1) can be written explicitly as follows:

$$\begin{pmatrix} \dot{I}_{s\alpha} \\ \dot{I}_{s\beta} \\ \dot{\Phi}_{r\alpha} \\ \dot{\Phi}_{r\beta} \end{pmatrix} = \begin{pmatrix} -\lambda & 0 & \frac{k}{T_r} & \omega_{rotor}k \\ 0 & -\lambda & -\omega_{rotor}k & \frac{k}{T_r} \\ \frac{L_m}{T_r} & 0 & -\frac{1}{T_r} & -\omega_{rotor} \\ 0 & \frac{L_m}{T_r} & \omega_{rotor} & -\frac{1}{T_r} \end{pmatrix} \begin{pmatrix} I_{s\alpha} \\ I_{s\beta} \\ \Phi_{r\alpha} \\ \Phi_{r\beta} \end{pmatrix} + \begin{pmatrix} \frac{1}{\sigma L_s} & 0 \\ 0 & \frac{1}{\sigma L_s} \\ 0 & 0 \\ 0 & 0 \end{pmatrix} \begin{pmatrix} V_{s\alpha} \\ V_{s\beta} \end{pmatrix} \tag{2}$$

Where:  $\lambda = \frac{1}{\sigma} \left( \frac{R_s}{L_s} + \frac{R_r}{L_r} (1 - \sigma) \right)$ ,  $\sigma = 1 - \frac{L_m^2}{L_s L_r}$ ,

$$k = \frac{L_m}{\sigma L_s L_r}, T_r = \frac{L_r}{R_r}$$

The electromagnetic torque equation is expressed as:

$$C_{em} = \frac{3}{2} p \frac{L_m}{L_r} (\Phi_{r\alpha} I_{s\beta} - \Phi_{r\beta} I_{s\alpha}) \tag{3}$$

The mechanical equation is expressed as:

$$\frac{d\Omega_r}{dt} = (C_{em} - C_r - f \cdot \Omega_r) / J \tag{4}$$

Table 1 shows the symbols used in this article.

TABLE 1  
TABLE OF SYMBOLS

$I_{s\alpha}, I_{s\beta}$	$(\alpha, \beta)$ axis stator current
$V_{s\alpha}, V_{s\beta}$	$(\alpha, \beta)$ axis stator voltage
$\Phi_{r\alpha}, \Phi_{r\beta}$	$(\alpha, \beta)$ axis rotor flux
$\overline{I}_s$	Space phasor of the stator currents expressed in the stator reference frame
$\overline{V}_s$	Space phasor of the stator voltages expressed in the stator reference frame
$\sigma$	Leakage coefficient
$T_r, T_s$	Rotor time constant, stator time constant
$\omega_{rotor}$	Rotor electrical speed
$\Omega_r$	Rotor speed
$L_m, L_s, L_r$	Mutual, stator and rotor inductance
$R_s, R_r$	Stator and rotor resistance
$p$	Poles number
$m$	The proportionality constant
$J$	Inertia moment
$f$	Viscous friction coefficient
$C_r, C_{em}$	Load torque, Electromagnetic torque

## 3 Direct Torque Control Principle

### 3.1 Direct Torque Control Description and Operation

The main idea behind the DTC of an IM supplied by a voltage source inverter (VSI) is the determination of the flux and torque directly and independently through selecting the optimal inverter switch states, while holding the flux and torque within their corresponding hysteresis bands respectively [12]. DTC avoids the use of current regulators, and pulse width modulation (PWM) generator.

Fig.1 shows the conventional DTC structure. The torque and flux calculations are done based on the voltage measurements and stator current through an estimator. These estimated values are compared to their reference values in order to use the errors as inputs to the hysteresis controllers. These controllers' outputs along with the flux location constitute the selector table inputs; whereas the output of this latter is the appropriate switching states vector applied to the VSI (see Table 2).

The switching states vector applied to VSI, indicated as  $(S_a S_b S_c)$  generates eight position

vectors  $(\vec{V}_1, \vec{V}_2, \dots, \vec{V}_8)$  where two correspond to the zero vector  $(S_a S_b S_c) = (111)$  or  $(000)$  as shown in Fig.2

### 3.2 Flux and Torque Estimation

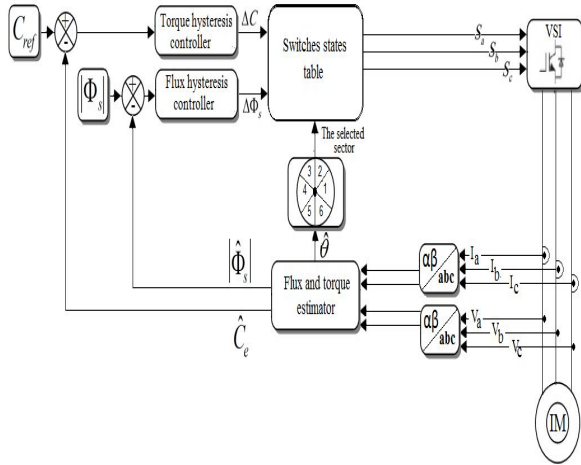


Fig.1 Basic Direct Torque Control Scheme of an Induction Motor with Voltage Source Inverter

TABLE 2  
OPTIMAL SWITCHING MODES TABLE

$\Delta\Phi_s$	$\Delta C$	Sector 1	Sector 2	Sector 3	Sector 4	Sector 5	Sector 6
1	1	110	010	011	001	101	100
	0	111	000	111	000	111	000
	-1	101	100	110	010	011	001
0	1	010	011	001	101	100	110
	0	000	111	000	111	000	111
	-1	001	101	100	110	010	011

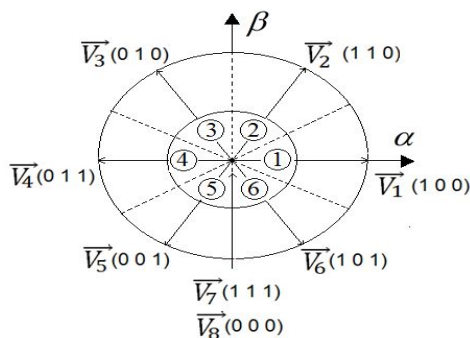


Fig.2 Stator Voltages Vectors Applied to the Voltage Source Inverter

Flux and torque equations are expressed based on the IM dynamic model in the stator reference frame,  $(\alpha, \beta)$  coordinates.

The flux equation can be written as:

$$\vec{\Phi}_s = \int_0^t (\vec{V}_s - R_s \vec{I}_s) dt \quad (5)$$

The flux components in the  $(\alpha, \beta)$  coordinates can be expressed as:

$$\Phi_{s\alpha} = \int_0^t (V_{s\alpha} - R_s I_{s\alpha}) dt \quad (6)$$

$$\Phi_{s\beta} = \int_0^t (V_{s\beta} - R_s I_{s\beta}) dt \quad (7)$$

The stator flux module is:

$$|\hat{\Phi}_s| = \sqrt{\Phi_{s\alpha}^2 + \Phi_{s\beta}^2} \quad (8)$$

The torque equation is:

$$\hat{C}_e = \frac{3}{2} p (I_{s\beta} \Phi_{s\alpha} - I_{s\alpha} \Phi_{s\beta}) \quad (9)$$

## 4 The Proposed Artificial Neural Networks Selector Table

### 4.1 Artificial Neural Networks Overview

ANN emulate the biological neural networks in their structure as well as in their way of working.

The neuron as shown in Fig.3-(a) represents the basic processing element in the nervous system. It receives impulses from others neurons, through elements called dendrites. Before reaching the dendrites, each impulse passes through synapses which are junctions between two given nerve cells. The junction gap is filled with chemicals called neurotransmitters; their role is accelerating or decelerating the flow of impulses. All of these impulses are summed in the nucleus afterwards. Then, they are transmitted through the axon, in order to feed other neurons.

The artificial neuron as illustrated in Fig.3-(b) receives the impulses multiplied by synaptic weights, afterward; a node sums the weighted input impulses. The accumulated signals, flow through the activation function to the output. The mathematical form of a neuron is represented by [13]:

$$Y = \theta \left( \sum_{i=1}^n W_{1,i} X_i - b \right) \quad (10)$$

The ANN which is an interconnection of artificial neurons, can be represented as shown in Fig.4

### 4.2 Structure of Direct Torque Control's Selector Table based on ANN

In the aim of avoiding high ripples at the level of torque and flux, which are among DTC's main disadvantages, the conventional selector table was replaced by an intelligent one based on ANN. The proposed DTC structure is presented in Fig.5.

The ANN selector table inputs are the outputs of the hysteresis controller of the flux and torque respectively, and the flux location, whereas the outputs are the three elements of the switching states vector. Thus the ANN selector table has three inputs and three outputs, i.e. three neurons in the input layer and three neurons in the output layer respectively. The architecture chosen for the ANN based DTC is 3-4-4-3. In order to obtain a robust ANN, the characteristics in Table 3 are chosen.

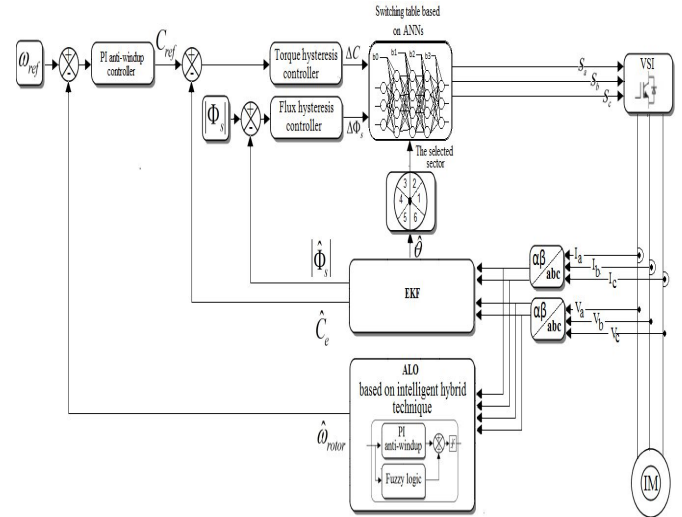


Fig.5 The proposed DTC's structure

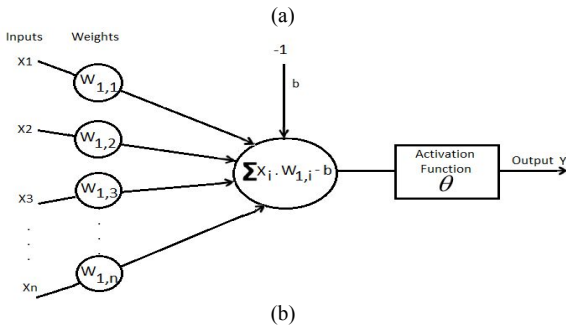
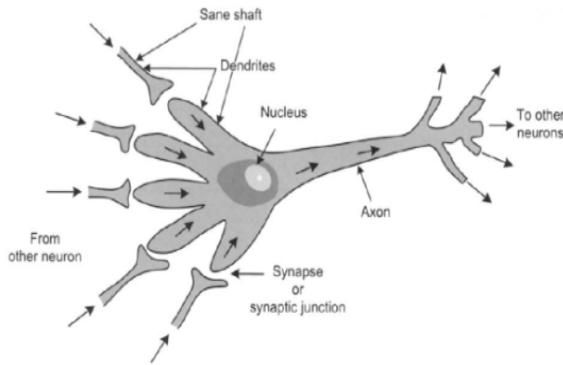


Fig.3 Structure of: a) Biological neuron b) Artificial neuron

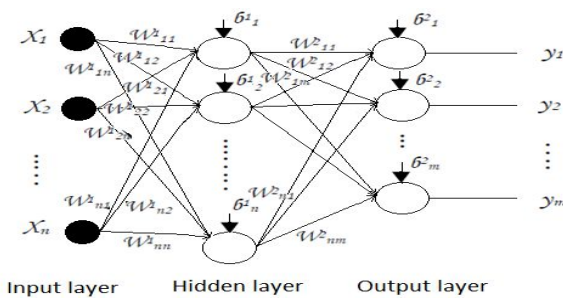


Fig.4 Artificial neural networks structure

TABLE 3

ARTIFICIAL NEURAL NETWORKS SELECTOR TABLE CHARACTERISTICS

Artificial neural networks characteristics	
ANN Architecture	Feedforward backpropagation
Learning algorithm	Levenberg marquardt
Number of neurons in the input layer	3 neurons
Number of neurons in the hidden layers	4 neurons in each layer
Number of neurons in the output layer	3 neurons
Type of activation functions	Tangent sigmoid and purelin
Goal error	10 <sup>-3</sup>
Epochs number	200

### 5 PI Anti-Windup Speed Controller

In order to correct the integral action, the PI speed controller is replaced by a PI anti-windup controller based on the back calculation method according to the scheme in Fig.6 [14]

The integral action correction is based on the saturation error  $u_e$  and the anti-windup gain  $K_s$ ,

$$\text{Where: } u_e = u_{in} - u_{out} \tag{11}$$

$u_{in}$  and  $u_{out}$  are the input and the output of the saturation component respectively.

### 6 Dual Observer

Using hardware observers induces several issues, to cite a few: additional cost, heavy volume addition, and location problems. In order to eliminate these problems, an intelligent dual observer is proposed; this new observer merges ALO based on hybrid technique for adaptation mechanism and EKF.

### 6.1 Rotor Speed Estimation using Adaptive Luenberger Observer based on Fuzzy-PI Anti-Windup Hybrid Technique for Adaptation Mechanism

The ALO is a deterministic type of observer which reconstructs the state of the rotor speed and the flux components, from the stator voltages and currents measurement. In this work, the ALO is used for the IM rotor speed estimation, based on fuzzy-PI anti-windup hybrid technique for adaptation mechanism.

The diagram of the ALO structure is shown in Fig. 7:

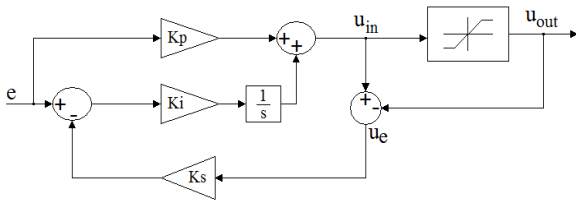


Fig.6 PI anti-windup based on back calculation method

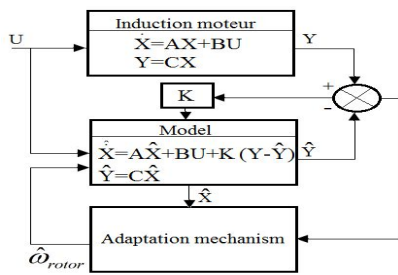


Fig.7 Structure of the adaptive Luenberger observer

Where:  $X = [I_{sa} \quad I_{sb} \quad \Phi_{ra} \quad \Phi_{rb}]^T$

$$U = [V_{sa} \quad V_{sb}]^T, Y = [I_{sa} \quad I_{sb}]^T$$

$$(Y - \hat{Y}) = [I_{sa} - \hat{I}_{sa} \quad I_{sb} - \hat{I}_{sb}]^T = [e_{sa} \quad e_{sb}]^T$$

$$C = \begin{bmatrix} 1 & 0 & 0 & 0 \\ 0 & 1 & 0 & 0 \end{bmatrix}^T$$

A symbol with ^ is the equivalent of its estimated value.

A symbol with ' is the equivalent of its derived value.

$A, B$ , represent the matrices of the IM model in  $(\alpha, \beta)$  coordinates.

$K$  is the observer gain matrix, which is selected to ensure the robustness and the stability of the observer [15]. With  $K$  is given by:

$$K = \begin{bmatrix} K_1 & -K_2 \\ K_2 & K_1 \\ K_3 & -K_4 \\ K_4 & K_3 \end{bmatrix} \tag{12}$$

Where:

$$K_1 = (m-1) \left( \frac{1}{\sigma T_s} + \frac{1}{\sigma T_r} \right)$$

$$K_2 = -(m-1) \hat{\omega}_{rotor}$$

$$K_3 = (m^2 - 1) \left\{ \left( \frac{1}{\sigma T_s} + \frac{1}{\sigma T_r} \right) \frac{\sigma L_s L_m - L_m}{L_r} \right\} + \left\{ \left( \frac{1}{\sigma T_s} + \frac{1}{\sigma T_r} \right) \frac{\sigma L_s L_m}{L_r} (m-1) \right\}$$

$$K_4 = -(m-1) \frac{\sigma L_s L_m}{L_r} \hat{\omega}_{rotor}$$

In the aim of establishing a good compromise between stability and simplicity of the observer, the ALO equations are expressed based on the dynamic model of the IM in the stator reference frame [11]:

$$\dot{X} = AX + BU + K(Y - \hat{Y}) \tag{13}$$

$$\hat{Y} = C\hat{X} \tag{14}$$

In order to estimate the rotor speed, the adaptation mechanism is determined by Lyapunov theory. The observer error equation is expressed as follows:

$$\frac{de}{dt} = \frac{d}{dt}(X - \hat{X}) = (A - KC)e + \Delta A \hat{X} \tag{15}$$

Where:

$e$  is the error estimation of the stator current and rotor flux

$\Delta A$  is the error state matrix, with  $\Delta A$  is given by:

$$\Delta A = A - \hat{A} = \begin{bmatrix} 0 & 0 & 0 & k \Delta \omega_{rotor} \\ 0 & 0 & -k \Delta \omega_{rotor} & 0 \\ 0 & 0 & 0 & -\Delta \omega_{rotor} \\ 0 & 0 & \Delta \omega_{rotor} & 0 \end{bmatrix}$$

$$\Delta \omega_{rotor} = \omega_{rotor} - \hat{\omega}_{rotor}$$

Where:

$$k = \frac{L_m}{\sigma L_s L_r}$$

The following Lyapunov function is considered:

$$V = e^T e + \frac{(\Delta \omega_{rotor})^2}{\gamma} \tag{16}$$

Where  $\gamma$  is a positive coefficient. Based on the derivative of equation (16), the adaptation mechanism law for the estimation of the rotor speed based on a PI controller is expressed as follows:

$$\hat{\omega}_{rotor} = K_p (e_{Is\alpha} \hat{\Phi}_{r\beta} - e_{Is\beta} \hat{\Phi}_{r\alpha}) + \frac{K_i}{s} \int (e_{Is\alpha} \hat{\Phi}_{r\beta} - e_{Is\beta} \hat{\Phi}_{r\alpha}) dt \tag{17}$$

Where:  $K_p$  and  $K_i$  are positive constants.

### 6.1.1 Intelligent Hybrid Technique for adaptation mechanism

In order to improve the performance of the ALO observer, the PI controller which consists the adaptation mechanism is replaced by a powerful fuzzy-PI anti-windup hybrid controller as is represented in Fig.8, combining the advantages of both techniques; on one hand, the flexibility and ability of the fuzzy to regulate a system through human knowledge, without complete knowledge of its hidden dynamics [16]. Thus it is an efficient way to face incomplete information and imprecise knowledge. On the other hand, the correction of the integral action by the PI anti-windup.

#### a. Fuzzy logic controller

In Fig.9, the FL controller structure is represented.

Where:  $K_e$ ,  $K_{de}$  and  $K_{di}$  are the scale factors that change the FL controller sensitivity without changing its structure.

The inputs of the FL controller are the error  $e$  and the derived error  $de$ . The main parts of this controller are [11]:

- **Fuzzification:** the process responsible for guaranteeing the inputs compatibility with the fuzzy set representation, whereas through this phase the

crisp input variables  $e$  and  $de$  are converted to fuzzy linguistic values.

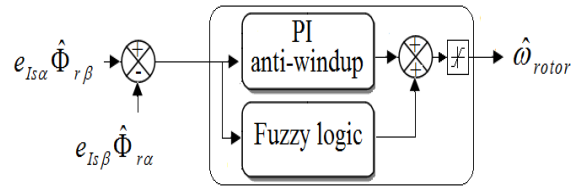


Fig.8 Intelligent hybrid technique for adaptation mechanism

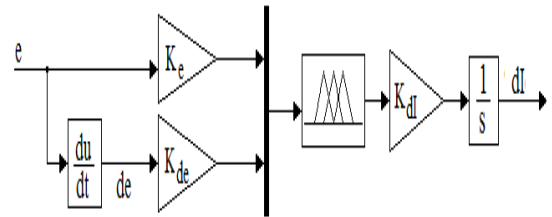


Fig.9 The fuzzy controller structure

- **Knowledge base:** it consists of two main parts:
  - The database represents the required information to achieve the FL process, for example, the fuzzy set representation of input-output variables and membership functions (MF).
  - The rule base which is expressed from expert knowledge based on the IF-THEN rules format. For example: IF  $e$  is (PB) and  $de$  is (NM) THEN  $di$  is (PS).
- **Inference engine:** is the process which performs the logical operations for FL control.
- **Defuzzification:** converts the fuzzy linguistic variables to a crisp variable output, which is  $di$  in this paper.

Among the multiple defuzzification methods that exist, the center of gravity defuzzification technique based on the inference strategy mamdani was chosen, in this paper.

For a FL controller design, the determination of the MF and the rules is necessary.

In this FL controller, the inputs  $e$  and  $de$  respectively, and output  $di$  have seven MF, these latter are mainly triangular as shown in Fig. 10

Linguistic variables are defined as {NB, NM, NS, Z, PS, PM, PB}: NB (Negative Big), NM (Negative

Medium), NS (Negative Small), Z (Zero), PS (Positive Small), PM (Positive Medium) and PB (Positive Big). The number of rules is  $7*7=49$ , and they are represented in Table 4.

**b. PI anti-windup controller**

The structure of the PI anti-windup controller used is similar to the one used and detailed above.

**6.2 Components Flux Estimation Estimation using the Extended Kalman Filter**

In the proposed sensorless DTC structure, the components flux of IM are estimated based on EKF.

The EKF is a stochastic observer used for state

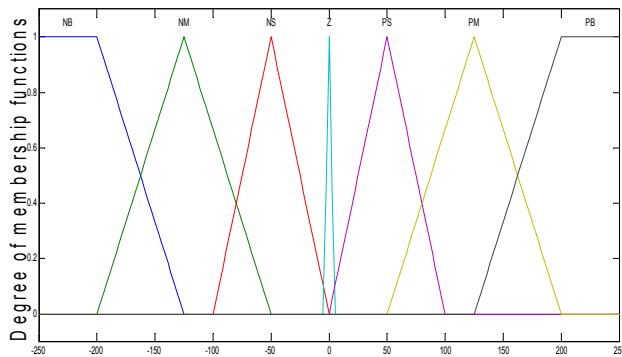


Fig.10 Membership functions used for the fuzzy logic controller

TABLE 4  
FUZZY RULES

<i>dl</i>	<i>e</i>						
	NB	NM	NS	Z	PS	PM	PB
	PB	Z	PS	PM	PB	PB	PB
	PM	NS	Z	PS	PM	PB	PB
<i>de</i>	PS	NM	NS	Z	PS	PM	PB
	Z	NB	NM	NS	Z	PS	PM
	NS	NB	NB	NM	NS	Z	PS
	NM	NB	NB	NB	NM	NS	Z
	NB	NB	NB	NB	NB	NM	NS

and parameters estimation of a non-linear dynamic system in real-time by using noisy signals that are distributed by random noise [15].

The calculation of the EKF outputs is performed following two main phases. In a first phase the states are predicted. In a second phase, they are continuously corrected with the help of a feedback correction term [17]. This latter is the product of the EKF gain and the difference between measured and estimated output signals. Based on this deviation,

the EKF provides an optimum output value at the next input instant.

Considering the system noise  $W$  and the measurement noise  $V$ , the dynamic behavior of the IM can be expressed under the following general form [18]:

$$\dot{x} = f(x, u) + W \tag{18}$$

$$y = h(x) + V \tag{19}$$

Where:

$$f(x, u) = \begin{bmatrix} -\lambda I_{sa} + \frac{k}{T_r} \Phi_{ra} + k \hat{\omega}_{rotor} \Phi_{r\beta} + \frac{1}{\sigma L_s} V_{sa} \\ -\lambda I_{s\beta} - k \hat{\omega}_{rotor} \Phi_{ra} + \frac{k}{T_r} \Phi_{r\beta} + \frac{1}{\sigma L_s} V_{s\beta} \\ \frac{L_m}{T_r} I_{sa} - \frac{1}{T_r} \Phi_{ra} - \hat{\omega}_{rotor} \Phi_{r\beta} \\ \frac{L_m}{T_r} I_{s\beta} + \hat{\omega}_{rotor} \Phi_{ra} - \frac{1}{T_r} \Phi_{r\beta} \\ 0 \end{bmatrix}$$

$$h(x) = [I_{sa} \quad I_{s\beta}]^T$$

In this case, the state vector becomes:

$$x = [I_{sa} \quad I_{s\beta} \quad \Phi_{ra} \quad \Phi_{r\beta} \quad \hat{\omega}_{rotor}]^T$$

In addition to states estimation which is the aim behind EKF, the problems and statistics concerning variations and noise are taken into consideration; covariance matrices  $Q, R, P$  of the system noise vector, measurement noise vector, and system state vector (x) respectively [15]. The covariance matrices  $Q, R$  are defined as follows:

$$Q = \text{cov}(W) = E\{WW^T\}; R = \text{cov}(V) = E\{VV^T\} \tag{20}$$

Therefore, the flux components can be estimated from the following discretized EKF algorithm based on the below dynamic model:

1) *Linearization*

$$F_k = \frac{\partial f(x_{k/k}, u_k)}{\partial x_k}; C_k = \frac{\partial h(x_k)}{\partial x_k} = \begin{bmatrix} 1 & 0 & 0 & 0 & 0 \\ 0 & 1 & 0 & 0 & 0 \end{bmatrix}$$

2) *Prediction / Estimation*

$$\hat{x}_{k+1/k} = f(x_{k/k}, u_k)$$

$$P_{k+1/k} = F_k P_{k/k} F_k^t + Q$$

3) *EKF gain*

$$K_{k+1} = P_{k+1/k} C_k^t [C_k P_{k+1/k} C_k^t + R]^{-1}$$

4) *Correction / Updating*

$$\hat{x}_{k+1/k+1} = \hat{x}_{k+1/k} + K_{k+1} (y_{k+1} - C_k \hat{x}_{k+1/k})$$

$$P_{k+1/k+1} = P_{k+1/k} - K_{k+1} C_k P_{k+1/k}$$

1) *Linearization*

Where:

$$F_k = \begin{bmatrix} 1 - T_s \lambda & 0 & T_s \frac{k}{T_r} & T_s k \hat{\omega}_{rotor} & 0 \\ 0 & 1 - T_s \lambda & -T_s k \hat{\omega}_{rotor} & T_s \frac{k}{T_r} & 0 \\ T_s \frac{L_m}{T_r} & 0 & 1 - T_s \frac{1}{T_r} & -T_s \hat{\omega}_{rotor} & 0 \\ 0 & T_s \frac{L_m}{T_r} & T_s \hat{\omega}_{rotor} & 1 - T_s \frac{1}{T_r} & 0 \\ 0 & 0 & 0 & 0 & 1 \end{bmatrix}$$

### 7 Simulation Results and Discussion

Many simulation tests were done based on the proposed powerful sensorless ANN-DTC based on hybrid observer and intelligent hybrid technique for adaptation mechanism of an IM. Simulations have been achieved using matlab/simulink. The IM parameters are presented in the Table 5 as follows:

TABLE 5  
INDUCTION MOTOR PARAMETERS

Rated power	3 Kw
Voltage	380V Y
Frequency	50 Hz
Rated speed	1440 rpm
Poles number	2
Stator resistance	2.2 Ω
Rotor resistance	2.68 Ω
Stator inductance	0.229 H
Rotor inductance	0.229 H
Mutual inductance	0.217 H
Inertia moment	0.047 Kg.m <sup>2</sup>
Viscous friction coefficient	0.004(N.m.s)/rad

#### 7.1 Functioning in one Motor Rotation Direction without Load Torque Disturbance

Figures 11 (a, b, c, d, e, f) show the motor’s simulation results while operating at speed 100 rad/s. These figures present reduced ripples at the level of flux, stator phase current and torque, and an excellent speed pursuit as well.

#### 7.2 Functioning in both Motor Rotation Directions with application of load torque disturbance

Figures 12 (a, b, c, d) represent motor’s simulation results while functioning at speed 100 rad/s until 1.5s, the speed is reversed to -100 rad/s afterwards. A load torque of 10 N.m is applied between 0.7s and 1.2s. From these results, a very good dynamic performance is clearly observed in both motor

rotation directions, with a very quick rejection of the disturbance and with a neglected overshoot.

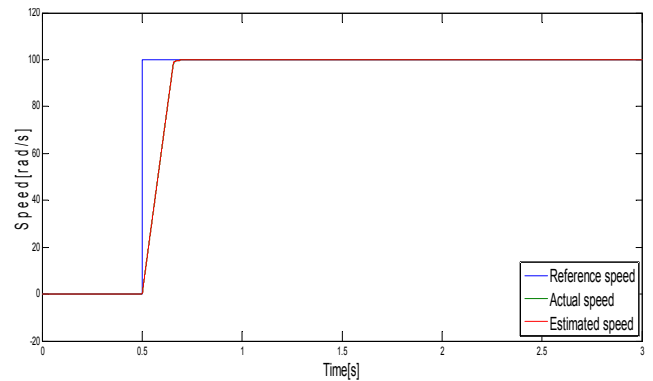
#### 7.3 Functioning at High Speed

The motor’s simulation results while operating at different high speeds which are 120, 150 and 135 rad/s are illustrated in figures 13 (a, b, c, d). These figures present a neglected overshoot even at start up of the highest speed of the motor and appropriate range values of the stator phase current and circular flux trajectory. Also a great speed observation is clearly remarkable.

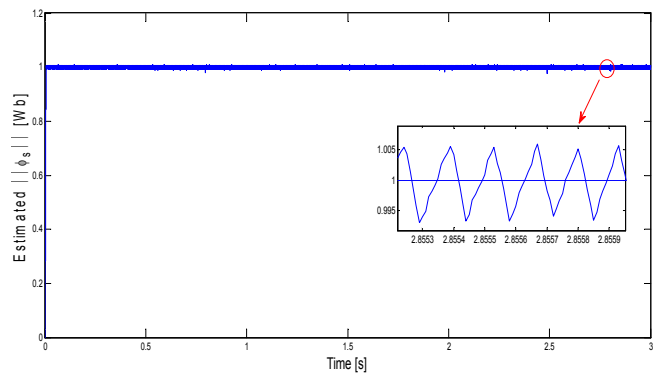
#### 7.4 Functioning at low Speed

Figures 14 (a, b, c, d) illustrate the motor’s performance while operating at different low speeds, which are 15, 25 and -10 rad/s. These figures show the circular flux trajectory, estimated flux and torque with minimal ripples.

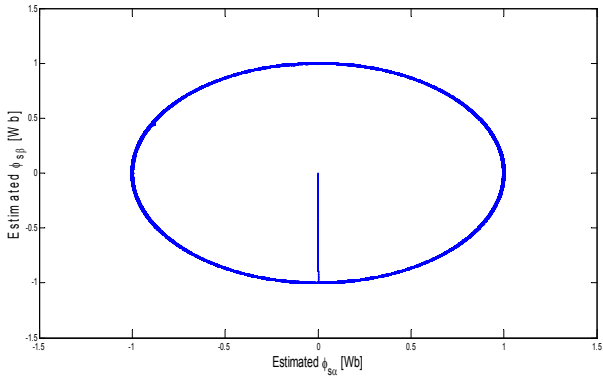
The new proposed sensorless hybrid system generates a powerful and efficient dynamic performance, which can be obviously deduced from the simulation tests above; minimal ripples at the level of the current, the flux and the torque, neglected overshoot, fast response, and perfect speed observation which is almost equal to zero.



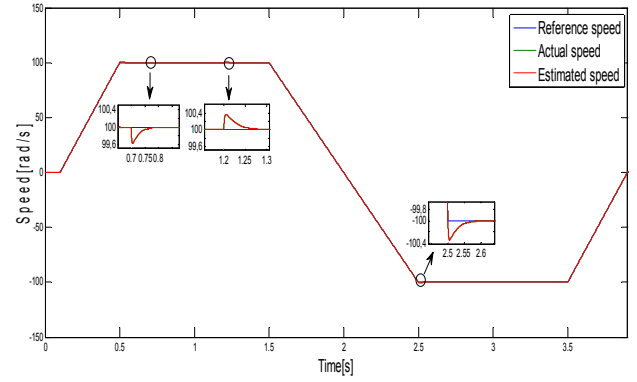
(a) Speed



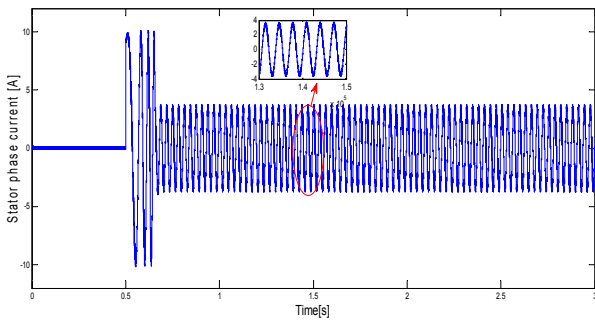
(b) Estimated stator flux



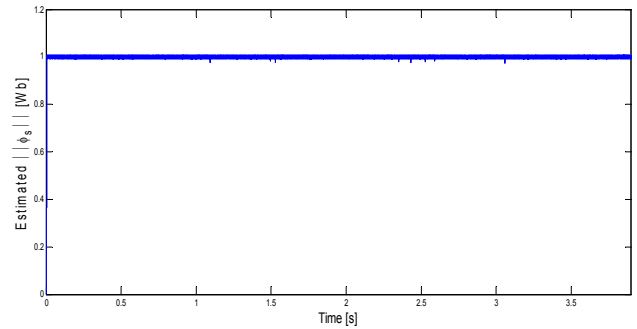
(c) Trajectory of Estimated stator flux components



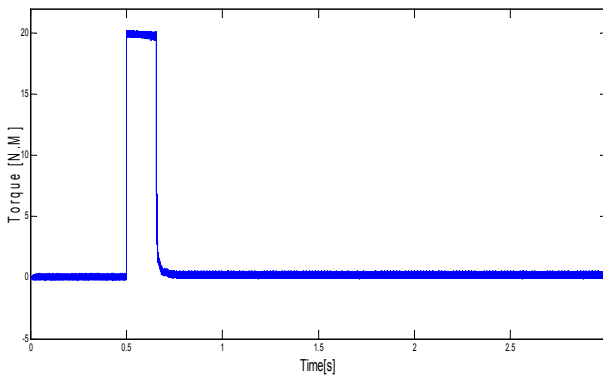
(a) Speed



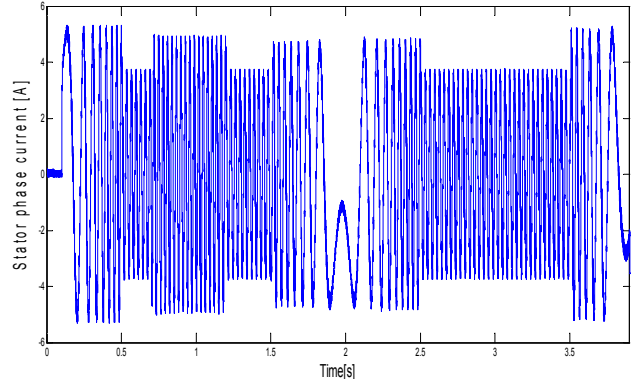
(d) Stator phase current



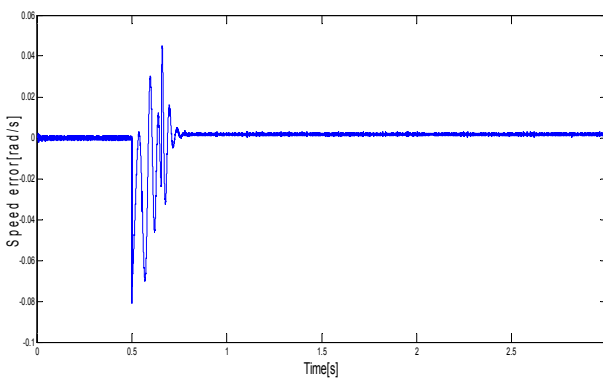
(b) Estimated stator flux



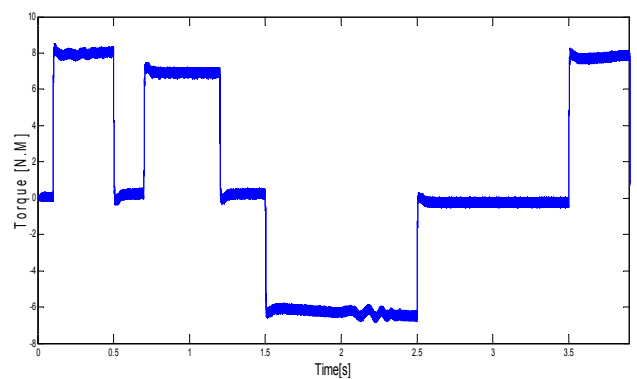
(e) Torque



(c) Stator phase current



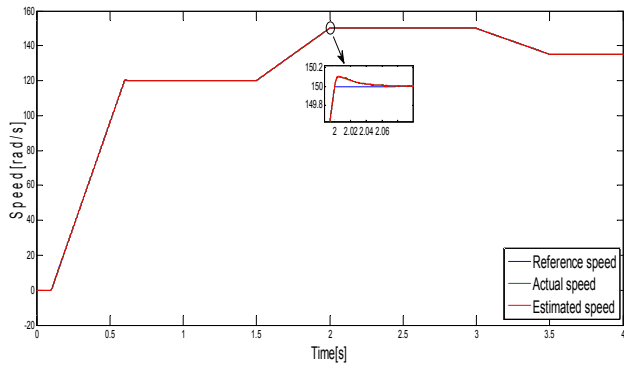
(f) Speed error



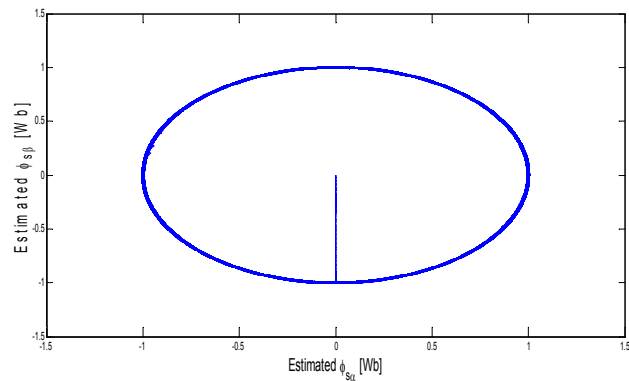
(d) Torque

Fig.11 Functioning in one motor rotation direction

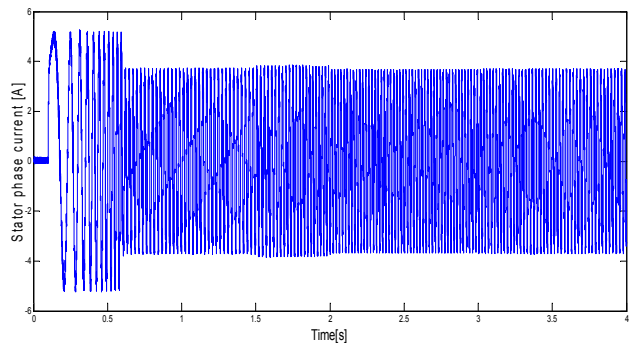
Fig.12 Functioning in both motor rotation directions with load torque



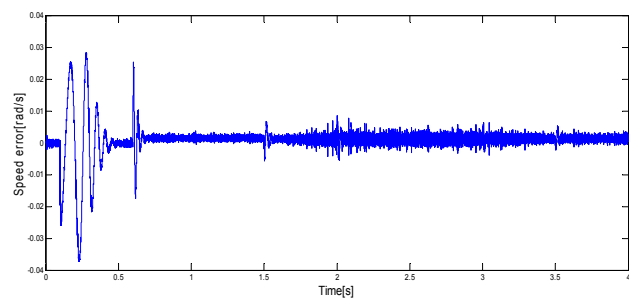
(a) Speed



(b) Trajectory of Estimated stator flux components

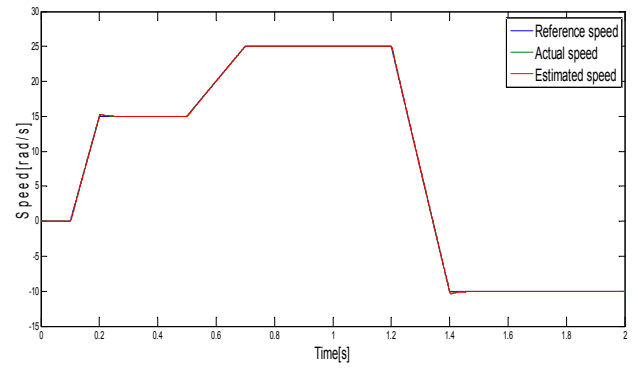


(c) Stator phase current

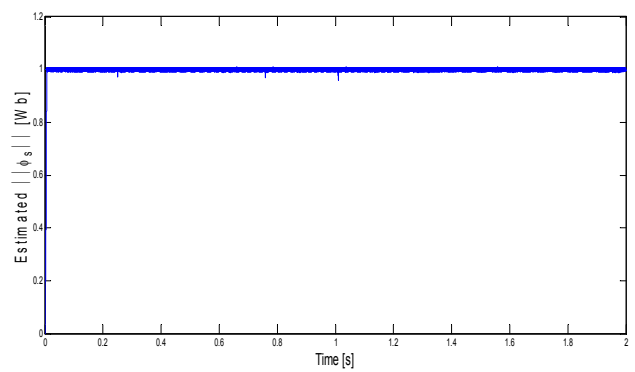


(d) Speed error

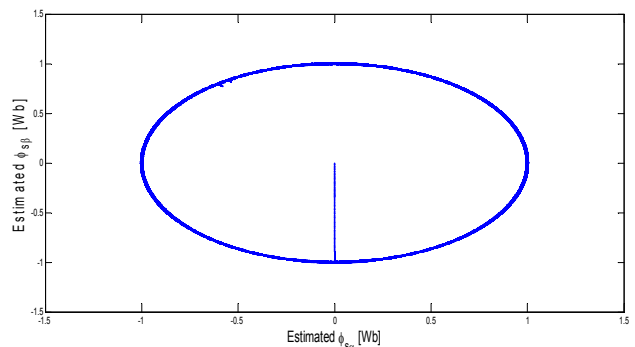
Fig.13 Functioning at high speed



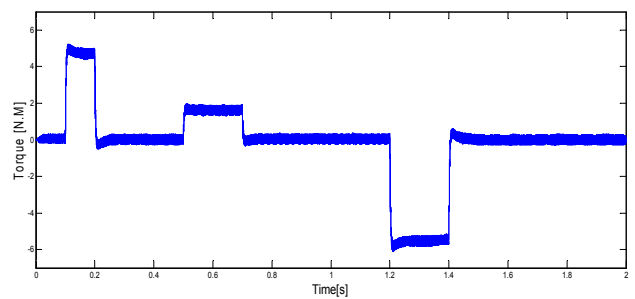
(a) Speed



(b) Estimated stator flux



(c) Trajectory of Estimated stator flux components



(d) Torque

Fig.14 Functioning at low speed

## 8 Conclusion

In this paper, a new sensorless ANN-DTC based on a hybrid observer combining ALO and EKF, and an intelligent hybrid technique combining FL and PI anti-windup techniques for adaptation mechanism of an IM is proposed. This system has proved many dynamic advantages at high, medium and low speeds, with and without load application, and in both motor rotation directions. These improvements are represented in the ability of the system to operate without a speed sensor, fast response, quick load torque rejection with neglected overshoots, minimized ripples at the level of the current, torque, flux, and excellent speed observation approaching zero.

### References:

- [1] M. Scarpino, *Motors for Makers: A Guide to Steppers, Servos, and other Electrical Machines*, Pearson Education, 2016.
- [2] H. Takahashi, T. Noguchi, A New Quick Response and High Efficiency Control Strategy of Induction Motor, *IEEE Transactions on Industry Applications*, Vol.22, No.5, 1986, pp. 820-827.
- [3] M. Depenbrock, Direct Self-Control DSC of Inverter Fed Induction Machine, *IEEE Transactions on Power Electronics*, Vol.3, No.4, 1988, pp. 420-429.
- [4] A. Taheri, Harmonic Reduction of Direct Torque Control of Six-Phase Induction Motor, *International Society of Automation (ISA)*, Vol.63, 2016, pp. 299-314.
- [5] W. Lin, D. Liu, Q. Wu, Q. Lu, L. Cui, J. Wang, Comparative Study on Direct Torque Control of Interior Permanent Magnet Synchronous Motor for Electric Vehicle, *International Federation of Automatic Control-Papers Online (IFAC)*, Vol.48, No.11, 2015, pp. 65-71.
- [6] A. Lokriti, I. Salhi, S. Doubabi, IM Direct Torque Control with No Flux Distortion and No Static Torque Error, *International Society of Automation (ISA)*, Vol.59, 2015, pp. 256-267.
- [7] J. Heaton, *Artificial Intelligence for Humans, vol 3: Neural Networks and Deep Learning*, Heaton Research, 2015.
- [8] M. Tariq, T.K. Bhattacharya, N. Varshney, D. Rajapan, Fast Response Antiwindup PI Speed Controller of Brushless DC Motor Drive: Modeling, Simulation and Implementation on DSP, *Journal of Electrical Systems and Information Technology (JESIT)*, Vol.3, No.1, 2016, pp. 1-13.
- [9] A. De La Guerra, Marco A. Arteaga-Pérez, A. Gutiérrez-Giles, P. Maya-Ortiz, Speed-Sensorless Control of SR Motors Based on GPI Observers, *Control Engineering Practice*, Vol.46, No.1, 2016, pp. 115-128.
- [10] C. Fahassa, Y. Sayouti, M. Akherraz, Improvement of the induction motor drive's indirect field oriented control performance by substituting its speed and current controllers with fuzzy logic components, *The 3rd International Renewable and Sustainable Conference (IRSEC), IEEE*, December 10-13, 2015, Marrakech, Morocco.
- [11] C. Fahassa, Y. Zahraoui, M. Akherraz, A. Bennassar, Improvement of induction motor performance at low speeds using fuzzy logic adaptation mechanism based sensorless direct field oriented control and fuzzy logic controllers (DFOC), *The 5th International Conference on Multimedia Computing and Systems (ICMCS), IEEE*, 29 September – 1 October, 2016, Marrakech, Morocco.
- [12] Ahmed M. Atallah, El Sayed F. El Tantawy, Direct Torque Control of Machine Side Multilevel Converter for Variable Speed Wind Turbines, *Energy*, Vol.90, No.1, 2015, pp.1091-1099.
- [13] A.K. Jain, Mao. Jianchang, K.M. Mohiuddin, Artificial Neural Networks: A Tutorial, *Computer – Special issue, Neural Computing, Companion issue to spring 1996 IEEE Computational Science and Engineering*, Vol.29, No.3, 1996, pp. 31– 44.
- [14] R.E. Precup, R.C. David, E.M. Petriu, M.B. Radac, S. Preitl, Adaptive GSA-Based Optimal Tuning of PI Controlled Servo Systems With Reduced Process Parametric Sensitivity, Robust Stability and Controller Robustness, *IEEE Transactions on Cybernetics*, Vol.44, No.11, 2014, pp. 1997 – 2009.
- [15] A. Glumineau, J. d. L. Morales, *Sensorless AC Electric Motor Control: Robust Advanced Design Techniques and Applications*, Springer, 2015.
- [16] L.A. Zadeh, Fuzzy Sets, *Information and Control*, Vol.8, No.3, 1965, pp. 338 – 353.
- [17] M. Koteich, *Modélisation et observabilité des machines électriques en vue de la commande sans capteur mécanique*, Ph.D. dissertation, CentraleSupélec, Paris-Saclay Univ., Saint-Aubin, France, 2016.
- [18] Md. Habibullah, D.D.C Lu, A Speed-Sensorless FS-PTC of Induction Motors Using Extended Kalman Filters, *IEEE Transactions on Industrial Electronics*, Vol.62, No.11, 2015, pp. 6765 – 6778.